

Lithiated Graphene Current Collector for Stable Anode-Free and Anode-Less Lithium Metal Batteries

Yi Ping Zheng,^[a] Xun Jian Hu,^[a] Xiao Ming Xu,^[b] Hai Feng Wang,^[b] Yu Long Sun,^[b] Ting Liu,^[a] Xian Bin Liu,^[a] Zi Ping Wu,^{*[a]} and Bao Yu Xia^{*[c]}

Anode-free and anode-less lithium (Li) metal batteries provide cell safety and afford maximum energy density. However, their practical applications are hampered by poor cycling performances. In this study, a composite of LiC₆ phase in highly reduced graphene (HrGO, LC-HrGO) is proposed as a current collector for Li metal plating. LC-HrGO provided homogenous plating sites and favorable conductivity, which facilitated Li metal plating with reduced nucleation barrier. The LiC₆ in composite is not easily delithiated, and the HrGO is not easily lithiated. The

obtained anode-free batteries based on the LC-HrGO current collector showed a capacity retention of 60% after 100 cycles, and the corresponding anode-less batteries indicated a stable specific capacity of 134.5 mAh g⁻¹ after 250 cycles and a remarkable rate capacity of 130.1 mA h g⁻¹ at 5 C. The work provides valuable concepts for fabricating promising current collectors towards Li metal batteries and beyond for high-level services.

Introduction

Lithium (Li) metal is known for its high theoretical specific capacity (3860 mAh g⁻¹) and low potential (-3.04 V versus the standard hydrogen electrode) among all feasible anode materials. However, Li metal tends to plate in needle-like or dendritic form during charging/discharging processes, possibly causing internal short circuit.^[1,2] Moreover, excess Li metal is used as the anode to prolong lifespan in most studies, leading to possible fire and explosion.^[3,4] Thus, plating and stripping Li metal on bare current collector at charging/discharging for anode-free Li metal batteries (AFLMBs) or decreasing the amount of Li metal in anode for anode-less Li metal batteries (ALLMBs) has attracted increasing attentions.^[5]

AFLMBs and ALLMBs possess low anode advantage that could enhance safety and energy density, but achieving long cycle remains a difficult challenge. The most important issue is that Li ions tend to aggregate on surface rather than interior of the current collector, leading to the growth of Li dendrites, which increase safety issue and lowers the energy density of batteries.^[6] Several strategies have been proposed, including

electrolyte engineering,^[7] building artificial solid electrolyte interphase (SEI),^[8] introducing solid state electrolyte,^[9-11] and optimizing three-dimensional (3D) skeleton hosts,^[12] to address these challenges. The 3D hosts are expected to accommodate Li plating/stripping and volume fluctuations due to their abundant interconnecting structures.^[13] The Li flux can be homogenized effectively by the unique surface chemistry of the hosts, and the nucleation potential barrier of Li could be decreased considerably.^[14] Tang et al. developed a 3D foam copper loading nickel-cobalt alloy and zinc oxide particles that could mitigate the volume expansion issues during Li plating/stripping.^[15] Lu's group developed a composite anode with uniform N doping by etching carbon cloth, which extends the cyclic performance of batteries.^[16] However, chemical modifications suffer from undesired electrochemical reactions that could decrease the conductivity of the anode.^[17] In addition, the drawbacks of homogeneity of these lithophilic components in the hosts cannot be easily overcome, leading to deteriorated electrochemical performance.^[18] Most of the approaches are complicated and time-consuming, and they involve toxic reagents, thereby limiting their practical applications.^[19] Therefore, developing an effective and prospective approach remains challenging for long lifespan AFLMBs or ALLMBs.

In this study, we report a composite of molten Li on highly reduced graphene (HrGO) as a current collector through metallurgical technique to fabricate dendrite-free AFLMBs and ALLMBs. The produced LiC₆ and HrGO composite (LC-HrGO) provides homogenous plating sites and favorable conductivity, which is the powerful driving force to facilitate Li metal plating with reduced nucleation barrier and ohmic impedance, resulting in enhanced kinetic condition. In addition, the obtained LiC₆ is not easily delithiated, and the HrGO is not easily lithiated. The assembled LC-HrGO | Li showed an excellent coulombic efficiency (CE) of 99.1% after 250 cycles at a current density of 0.5 mA cm⁻². The corresponding LC-HrGO | LiFeO₄ (LFP) AFLMB demonstrated a capacity retention of 60% after 100 cycles.

[a] Y. Ping Zheng, X. J. Hu, T. Liu, X. Bin Liu, Prof. Z. P. Wu
Faculty of Materials Metallurgy and Chemistry, Jiangxi University of Science and Technology (JXUST), 86 Hongqi Road, Ganzhou 341000, China
E-mail: wuziping724@jxust.edu.cn

[b] X. M. Xu, H. F. Wang, Y. L. Sun
Jiangxi Anchi New Energy Technology Co., Ltd, 128 Xingye Avenue, Shangrao 334000, China

[c] Prof. B. Y. Xia
Key Laboratory of Material Chemistry for Energy Conversion and Storage (Ministry of Education), Hubei Key Laboratory of Material Chemistry and Service Failure, Wuhan National Laboratory for Optoelectronics, School of Chemistry and Chemical Engineering, Huazhong University of Science and Technology (HUST), 1037 Luoyu Road, Wuhan 430074, China
E-mail: byxia@hust.edu.cn

 Supporting information for this article is available on the WWW under <https://doi.org/10.1002/batt.202400144>

After Li metal was supplemented in the current collector, the LC-HrGO@Li||Li showed a voltage hysteresis lower than 19.2 mV after 2100 h, with a current density of 1 mA cm⁻² and a capacity of 1 mAh cm⁻². Accordingly, the corresponding LC-HrGO@Li||LFP ALLMB suggested a stable specific capacity of 134.5 mAh g⁻¹ even after 250 cycles, and the anode-less cells had a remarkable rate capacity of 130.1 mA h g⁻¹ at high current rate (C-rate, 5 C). This work proposed an effective AFLMB and ALLMB fabrication that can significantly promote further development of their safety issues and electrochemical performances.

Experimental

The fabrication of HrGO and LC-HrGO. The graphene oxide (GO) with concentration of 20 mg ml⁻¹ was first fabricated using modified Hummer's method. And the GO film was then fabricated through slurry coating technology followed drying. The obtained GO film first reduced at 80 °C in HI and subsequently transferred into graphitization furnace to heat at temperature of 2800 °C for HrGO with complete reducing. Finally, the molten Li metal was poured into the HrGO in an argon-filled glove box (Mikrouna Shanghai Company Ltd). As a consequence, the yellow LC-HrGO can be fabricated. The total amount of Li pre-introduced into the LC-HrGO can be calculated according to the pouring before and after (Table S1).

The cathode electrode fabrication. The slurry-based technique was used to fabricate cathode electrodes of LFP and LiNi_{0.8}Co_{0.1}Mn_{0.1}O₂ (NCM811). Al foil with 12 µm thick was used as current collector. The polyvinylidene fluoride (PVDF, Arkema, France) and Super P carbon (Timcal, Switzerland) were employed as binder and conductive additive respectively. The slurries were prepared by mixing LFP (NCM811): PVDF: SPC in weight ratio of 80:10:10, which were dissolved into N-methyl-2-pyrrolidone (Tianjin Damao). Afterwards the mixture was stirred at room temperature for 8 h. The obtained slurries were coated on Al foil then dried at 120 °C for 2 h. Finally, the dried electrodes were tailored as per the requirements for cells assembling. The mass loading of the cathode active materials is 5 mg cm⁻².

Fabrication and performance measurement of batteries. The coin-type (CR 2032) half cells and full cells were assembled in an argon-filled glove box, and Cu foil, HrGO and LC-HrGO or plating Li metal on them were used as reference electrode for AFLMBs and ALLMBs. The solution of LiTFSI (1 M) in 1,3-dioxolane (DOL) and 1,2-dimethoxyethane (DME) mixed at a volume ratio of 1:1 with 1% LiNO₃ was employed as electrolyte for half cells and symmetrical cells. In addition, the solution of LiPF₆ (1.0 M) in diethyl carbonate (DEC) and ethylene carbonate (EC) mixed at a weight ratio of 1:1 was employed as electrolyte for full cells. The polyethylene (2400, Celgard, 20 µm) film was used as separator. The electrochemical performances of obtained batteries were tested on Neware battery tester. The galvanostatic charge/discharge was carried out in 2.5–4.0 V (vs. Li/Li⁺) for LFP electrodes and 3.0–4.3 V (vs. Li/Li⁺) for NCM811 electrodes. The batteries were tested at C-rate of ~0.1 C (the current density of 1 C is ~150 mA h g⁻¹ for LFP, and ~190 mA h g⁻¹ for NCM811). Cyclic voltammetry (CV) was performed on a standard electrochemical instrumentation (CHI 760E) with a scanning rate is 0.1 mV s⁻¹. The electrochemical impedance spectroscopy (EIS) tests were also conducted on the electrochemical station over a frequency range from 100 kHz to 0.01 Hz.

Material characterization. The morphologies of the obtained electrodes were investigated by field-emission scanning electron

microscopy (SEM, Supra 55 ZEISS). X-ray photoelectron spectroscopy (XPS, AxisUltraDld, Japan) was performed to probe Li and other elements in the electrodes and SEIs. The samples were immersed in DOL for 0.5 h and then dried to the electrolyte before the test. The composition of SEI at different thicknesses was analyzed using argon ion to etch the surface. The crystalline structures of the samples were tested by X-ray diffraction (XRD, PANalytical X'Pert instrument). In-situ images of Li metal plating were captured by an optical microscope.

Density functional theory (DFT) calculation. DFT was used to optimize the structure of the model and investigate the electronic structure of LiC₆ and graphene. The calculation is based on the projected augmented wave (PAW) method performed by Dmol³.^[20] GGA-PBE was employed to describe the exchange correlation between core electrons and valence electrons.^[21] A 15 Å vacuum layer was established along the c axis to avoid interlayer interaction. A double-numerical basis set was employed with polarization function (DNP) by using a real-space cutoff radius of 4.1 Å and a wave function smearing energy of 0.005 Ha. The Brillouin zone was sampled by Monkhorst–Pack method with 3×3×1 and 7×7×1 k-point grids for structural optimization and electronic structure calculation, respectively. The force and energy were 1×10⁻⁵ eV and 0.01 eV Å⁻¹, respectively.^[22,23] The geometric optimization was considered to be convergent. In addition, the binding energy between the HrGO (LC-HrGO) and Li also has been calculated based on the DFT.

Results and Discussion

A graphene oxide (GO) film was fabricated by chemical reduction and thermal reduction on basis of the authors' previous works.^[24,25] Then, the obtained film was placed in a graphitizing furnace and annealed for 2 h at 2800 °C under vacuum conditions. The color of the as-prepared GO film changed completely after heat treatment with ultrahigh temperature (Figure S1). After annealing, the reduction degree of HrGO considerably improved, and most of the defects were repaired (Figure 1a left and middle). Being directly wetted by the molten Li was extremely easy because of its excellent lithiophilicity. The color evolution from black to yellow indicated that the molten Li can be rapidly intercalated into HrGO (Figure 1a right). And the thickness of the LC-HrGO has negligible change compared to that of the HrGO (Figure S2). Due to the Gibbs free energy for the intercalation reaction between Li and HrGO is -10.59 KJ mol⁻¹. The formation of LiC₆ (Li+6 C→LiC₆) is thermodynamically spontaneous processes as Li contact with HrGO.^[26] In addition, the lithiated process is occurred at high temperature, and thereby the LiC₆ can be more easily obtained as HrGO immersed into molten Li. The XRD pattern (Figure 1b) indicated that the obtained composite is HrGO and LiC₆ phase. The characteristic sharp peak indicating the HrGO and LiC₆ phases demonstrated excellent crystallinity. And the LiC₁₂ and Li₂C₂ appeared in the electrode (Figure S3) may be the de-intercalated and intercalated behaviors for Li ion.^[12] The G-band at ~1580 cm⁻¹ is associated with tangential modes in pure sp² hybridized graphitic carbon, and the D-band at ~1360 cm⁻¹ is due to disordered sp³ type defects. The ratio of intensities of the G and D bands (I_G/I_D) in Figure 1c is a crude measure of the perfection of HrGO and LC-HrGO. The infinite I_G/I_D

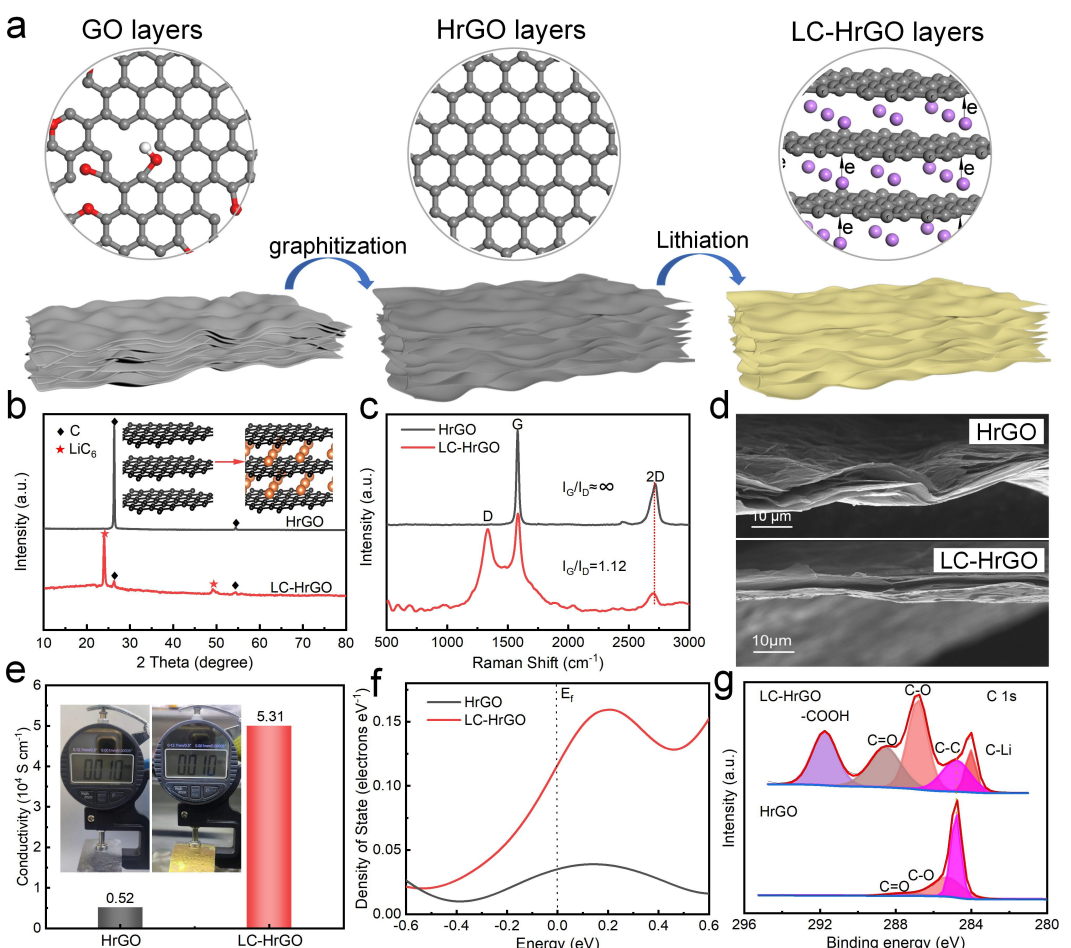


Figure 1. (a) The fabrication of LC-HrGO processes and their corresponding atomic structure, (b) the XRD patterns, (c) Raman spectrum, (d) cross-section images, (e) electrical conductivity, (f) the density and partial orbital density of states, and (g) high-resolution XPS spectra of C 1s for HrGO and LC-HrGO.

I_D indicated perfect crystallization of the HrGO after ultrahigh temperature treatment, which suggest the conjugated structure has been completely repaired at graphitization treatment. Thereby the electrons can be transferred quickly by the HrGO. However, the I_G/I_D decreased sharply as the Li intercalated into the HrGO, the decreased I_G/I_D suggested that the HrGO lattice could be distorted after Li insertion. And the conjugated structure would be destroyed and defects increased significantly. Due to the Li metal in the LC-HrGO has a higher electron transfer capability than that of the HrGO, the electrons also can be transferred quickly by the composite. The results were corresponding to the followed conductivity measurement and density of state calculation.

The as-obtained LC-HrGO remained intact under arbitrary bending (Figure S4), and the film became smoother than the HrGO film (Figure 1d), indicating its structural flexibility and uniformity for applications. The LC-HrGO film (Movie S1) showed inactivity in electrochemical reaction. The LC-HrGO and HrGO films showed very low specific capacity when used as anode for charging/discharging (Figure S5). The results indicated that LC-HrGO is a potential candidate as a current collector for plating and striping for Li metal. Electrical conductivity is another important factor for current collectors in

electrochemical reaction. Figure 1e shows that the electrical conductivity of the LC-HrGO film increased significantly ($5.31 \times 10^4 \text{ S cm}^{-1}$) after intercalating Li atoms in HrGO ($0.52 \times 10^4 \text{ S cm}^{-1}$). Compared with the HrGO, the thickness demonstrated negligible change after intercalating Li atoms (Figure 1e inset). The increased conductivity of the HrGO may be ascribed to the repairing of defects and recovering of conjugated structures.^[27] The density of states (DOS) and partial orbital density of states (PDOS) for LC-HrGO were calculated in accordance with DFT to explore the reason behind the ultrahigh conductivity. Compared with that of the HrGO, the Fermi level of LC-HrGO shifted towards the conduction band, resulting in a wider DOS of the conduction band, and enhanced the electron delocalization (Figures 1f and Figure S6). The probability of electrons appearing near the Fermi level greatly increased.^[28] A significant electron shift from Li to C was observed in LiC₆. Therefore, the electronic conductivity of the LC-HrGO rapidly increased.

The surface electronic states of the obtained LC-HrGO were further investigated by XPS. The results confirmed the presence of O, C, and Li on the surface of the sample (Figure S7 and Figure 1g). The Li 1 s signal is assigned to the intercalating reaction after molten Li addition. The peaks at 283.75, 284.8,

286.75, 288.50, and 291.75 eV in the C 1s high-resolution spectra are attributed to the C–Li, C–C, C–O, C=O and –COOH bonds, respectively.^[29,30] The element contents obtained by XPS in the HrGO and LC-HrGO were analyzed. The C and O contents were determined to be 95.1% and 4.9% in HrGO. The C content decreased sharply (39.5%) and Li increased significantly (21.9%) in the LC-HrGO after Li intercalation. The appearance of C–Li further confirmed the existence of LiC₆ phase, which corresponded with the XRD results. The different intensity peak of C–C in HrGO and LC-HrGO indicated that the lattice integrity could be destroyed by Li insertion (Figure S8). And the appearance of the –COOH showed in the high-resolution XPS spectra maybe due to the oxidization of the Li metal formed on the defect site. The Li 1s moved into high binding energy direction corresponding to the changes (Figure S9).^[31] The

numerous internal defects provided abundant nucleation sites for subsequent Li plating when LC-HrGO was employed as the current collector.

The nucleation barrier is an important factor to evaluate the lithiophilic property. Figure 2a shows lower barrier for Li plating onto LC-HrGO (21.3 mV) than HrGO (56.4 mV) and Cu (134.6 mV) at a current density of 1 mA cm⁻². This result confirmed that LC-HrGO can effectively reduce the potential barrier for Li nucleation, may be because of the strong electrostatic adsorption between Li ions and LiC₆ phase.^[32] In addition, the abundant defects provided sufficient nucleation sites. A similar phenomenon occurred when different current densities were employed (Figure S10 and S11). The wetness of molten Li metal on the HrGO and LC-HrGO confirmed the lithiophilic property (Figure S12). It is well known that the

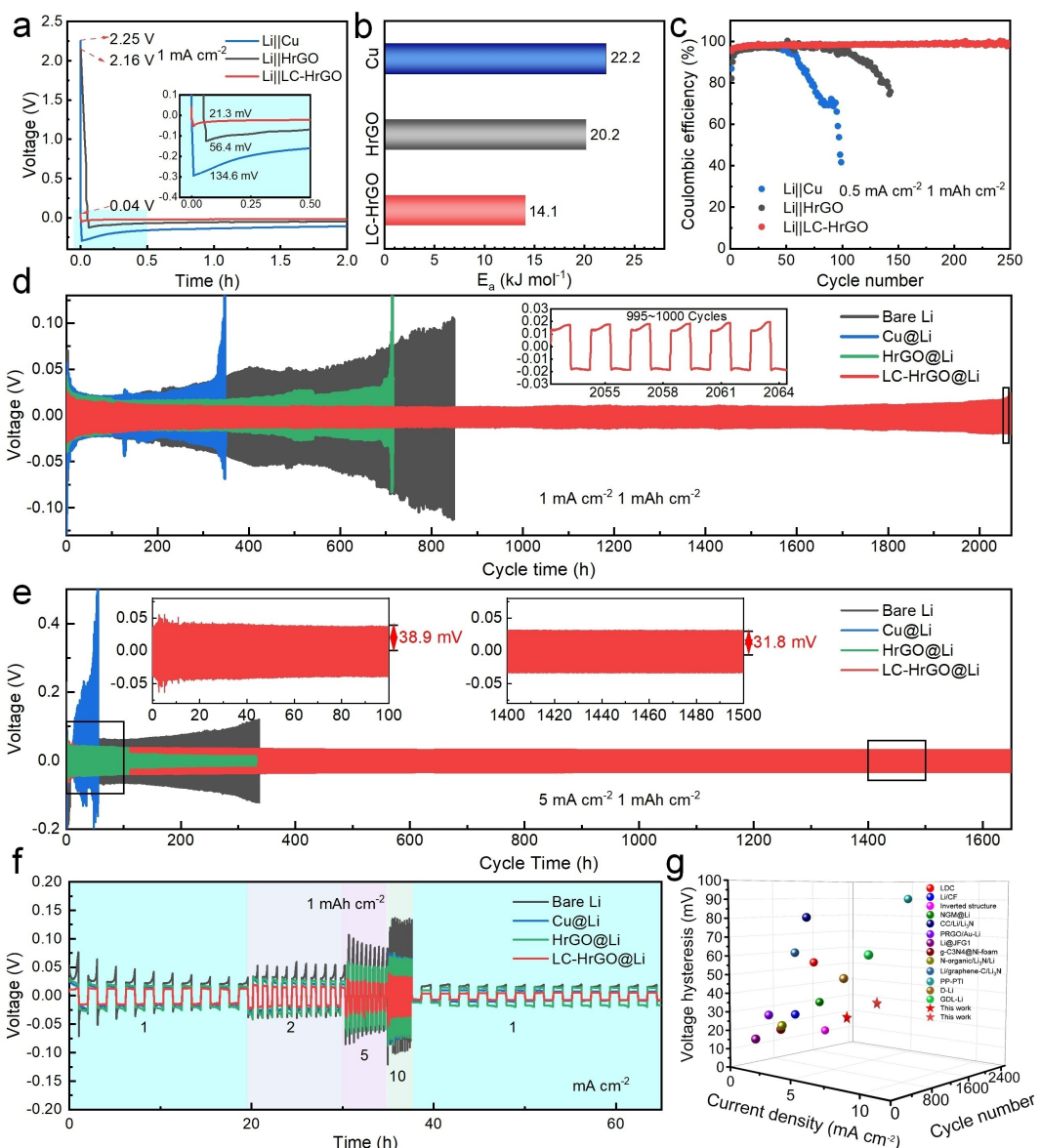


Figure 2. The electrochemical performances of the cells, (a) the nucleation barrier, (b) the activation energy for Li ions plating, (c) the coulombic efficiency of half cells, the galvanostatic cycling of a symmetric device at (d) a lower current density of 1 mA cm⁻² with a stripping/plating capacity of 1 mAh cm⁻² and (e) a higher current density of 5 mA cm⁻² with a stripping/plating capacity of 1 mAh cm⁻², and (f) rate performances of symmetric cells based on the Cu foil, HrGO and LC-HrGO, (g) the comparison of galvanostatic plating/stripping performances of the LC-HrGO current collector with previously reported materials.

wetness is related to their surface energy. The surface of the LC-HrGO has more defects than that of the HrGO and thereby it suggests high surface energy. In addition, the LC-HrGO also indicates high roughness. Thereby the LC-HrGO suggested better wetness for molten Li metal compared to the HrGO. Furthermore, the lower electrode potential of the LC-HrGO (0.04 V) than HrGO (2.16 V) and Cu (2.56 V) in the discharge curves demonstrated its potential as a candidate current collector for plating/stripping of Li metal. EIS between 295 K with 325 K was applied to explore the activation energy of the Li ion transferred across the anode interface. According to the Arrhenius formation,^[33] The LC-HrGO indicated the lowest activation energy (Figure S13, Figure 2b) among others (Tables S2–S4). In addition, the lower binding energy between the LC-HrGO and Li calculated by DFT is also corresponding to the results (Figure S14). The results suggested that the de-solvation process of the Li ion could be promoted with the assistance of LC-HrGO. Accordingly, the assembled Li||LC-HrGO showed a stable performance even after 250 cycles at a current density of 0.5 mA cm⁻², with a capacity of 1 mAh cm⁻² (Figure 2c). It should be noted that the Coulombic efficiency decreased, then increased, and decreased sharply for Li||Cu half cells. The reasons are contributed to the Li ions that tend to plate on dendrites rather than on smooth surface till the formation of the severe dendrites. As the current density increased, similar results were obtained (Figure S15a). Furthermore, the Li||LC-HrGO displayed a low polarization voltage in different cycles (Figures S15b–d). These results indicated that the lithiated reaction induced homogenous defects and increased conductivity for the HrGO. Therefore, the polarization and dendrites can be suppressed on the LC-HrGO during plating/stripping processes.

The galvanostatic charge/discharge cycling performances of symmetric cells with different collectors were investigated at different current densities and capacities. First, 4 mAh cm⁻² Li metal was plated on the Cu, HrGO, and LC-HrGO to measure their polarization. Figure 2d compares the voltage profiles of the symmetric cell with bare Li, Cu@Li, HrGO@Li, and LC-HrGO@Li counterparts at a current density of 1 mA cm⁻² and a capacity of 1 mAh cm⁻². The voltage hysteresis of bare Li, Cu, and HrGO gradually increased and became unstable, and their overpotential reached larger than 100 mV after 340–800 h. These results represented the aggravated polarization of these electrodes during the Li plating/stripping processes. By contrast, the voltage hysteresis of LC-HrGO was slightly higher at first and gradually reduced to a very low value of 19.2 mV after the first 20 cycles and maintained after over 2100 cycles. When the current density was increased to 2 mA cm⁻² with a capacity of 1 mAh cm⁻² (Figure S16), a stable cycling beyond 2000 cycles with a stable hysteresis was achieved in the LC-HrGO cell. However, the bare Li showed increased hysteresis in less than 50 h. In addition, the LC-HrGO cell stably operated in over 1650 cycles even with the further increase in current density of 5 mA cm⁻² with a capacity of 1 mAh cm⁻² (Figure 2e). Meanwhile, the voltage hysteresis of the bare Li showed a high voltage hysteresis in the later cycles. These results may be attributed to the abundant defects and excellent electrical

conductivity of LC-HrGO. Moreover, the current collector could provide sufficient active sites and electrons. The impedances shown in EIS curves (Figure S17, Table S5) corresponded with the voltage hysteresis results, and decreased polarization was demonstrated. The rate performances of the LC-HrGO@Li and other electrodes were investigated. As shown in Figure 2f, LC-HrGO@Li operated stably even when the current density was increased to 10 mA cm⁻² with a voltage hysteresis of only 33.7 mV. These results further suggested that the current density could be effectively dispersed by the LC-HrGO for excellent conductivity, and then fast electron transfer could be realized and abundant Li ions could be transferred. Finally, the remarkable rate capability of LC-HrGO could be obtained. To the best of the authors' knowledge, these values are the lowest voltage hysteresis values tested on modified current collectors for Li metal electrodes considering current density and cycles (Figure 2g and Table S6).

The morphology of the Cu, HrGO, and LC-HrGO as current collectors before and after cycling was studied to analyze the Li ion plating behavior (Figure 3). The pristine Cu foil showed a flat and compact surface, but the surface was found to be rough when magnified (Figure 3a). Li ions were easy to be plated on the uneven area for providing sufficient electrons. The surface of the HrGO showed wrinkles (Figure 3b). The defects further enhanced after being lithiated with the addition of molten Li metal (Figure 3c). After 4 mAh cm⁻² Li metal was plated on the current collector, the surface of the whole electrode became porous and fluffy (Figure 3d). The results indicated that abundant dendrites were present on the surface of the Cu foil. The plated Li metal on the HrGO was more compacted than that on Cu foil, may be because more pores on the surface and electron could be transferred quickly. However, dendrites formed as more Li was plated on the surface (Figure 3e). The plating behavior changed as Li was plated on the surface of LC-HrGO. Figure 3f shows dense surface with homogenous distribution of the Li metal and without dendrites or cracks observed on the surface. The morphology corresponded with that shown in the optical image (Figure 3f inset). The morphologies of the current collectors plated with Li metal with different current densities were investigated, and similar results were found (Figure S18). In addition, the plating behavior was investigated after several plating/stripping cycles. The surface of the LC-HrGO remained smooth after 70 cycles, but several dendrites were observed on the surface of the Cu foil and HrGO (Figure S19). These results indicated that sufficient electrons can be homogenously transferred, and Li ions can receive sufficient electrons and then be homogenously plated on the surface of LC-HrGO without dendrites.

The dynamic morphologies were studied through monitoring the Li metal plating processes by using an optical microscope *in situ*. Movie S2 shows the dynamic processes of the 4 mAh cm⁻² Li metal plated on Cu foil. The surface lost its metallic luster and became loose after being plated with 2 mAh cm⁻² Li metal (Figure 3g, and Figure S20a). Moreover, extreme dendrite growth was observed. Similar plating processes can be seen in Movie S3 when the current collector was

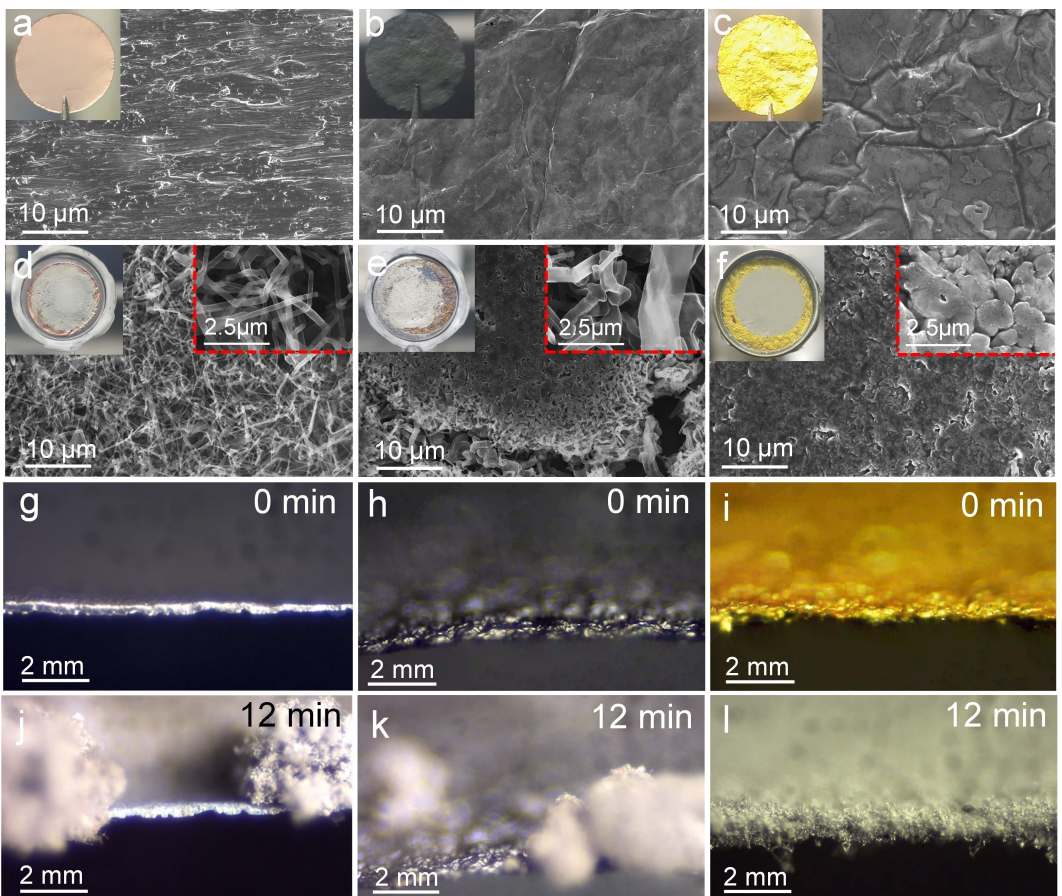


Figure 3. The SEM images and in situ optical observation, the as-prepared surface images of the (a) Cu foil, (b) HrGO and (c) LC-HrGO current collector (the inset images are their macroscopic morphologies), the surface images of the (d) Cu foil, (e) HrGO and (f) LC-HrGO current collector after plating 4 mAh cm^{-2} Li metal (the inset images are their macroscopic and enlarged morphologies), the cross-section images of the (g) Cu foil, (h) HrGO and (i) LC-HrGO current collectors before plating Li metal and the cross-section images of (j) Cu foil, (k) HrGO and (l) LC-HrGO after plating 4 mAh cm^{-2} Li metal.

replaced by HrGO. Figure 3h shows the surface morphology before plating. Dendrites appeared (Figure S20b) and then became extreme (Figure 3k) after plating. Figure 3i shows the yellow surface of LC-HrGO before plating, and the color became light grey when Li metal was plated on the pores of LC-HrGO (Figure S20c). The surface of the LC-HrGO remained flat until the end of plating (Figure 3l). Movie S4 shows the dynamic plating processes and the Li metal's homogenous growth on the surface. These results further confirmed the dendrite-free Li metal can be plated on the surface. The strong electronegativity of LiC_6 can homogeneously absorb the Li ions plated on the surface. Sufficient electrons can be transferred to the surface quickly for excellent conductivity.

The SEI layer formed on the surface of the anode has a significant effect on Li ion transport. The formation of the lithiated reaction products on the anode resulted in altered contents of the SEIs. Accordingly, the SEI composition was analyzed by XPS with Ar ion-sputtering depth profiling. The Cu foil and LC-HrGO as electrodes were plated/stripped for five cycles at a current density of 1 mA cm^{-2} with a capacity of 1 mAh cm^{-2} for analysis. The components of SEI on the surface of the electrode were analyzed at different depths through Ar-ion sputtering for 1 min. It comprises inorganic

(LiF , Li_2O , and Li_2CO_3) and organic ($\text{C}-\text{O}$ and $\text{C}=\text{O}$) components (Figure 4a, b and Figure S21). The LiF may be attributed to the reaction between the Li metal and the fluorine-containing electrolyte (LiPF_6), consistent with the results reported in other studies.^[34]

Oxides, such as Li_2O and Li_2CO_3 , were observed in the SEIs because of the oxygen in the electrolyte. LiF and Li_xPOF_y dominated in the F 1s spectra. The signal was stable as more surfaces were removed from the LC-HrGO and Cu electrode, accompanied by stable LiF and Li_xPyF_z in the F 1s signal (Figure 4a). The LiF signal intensities in LC-HrGO were higher than those in the SEI in the Cu electrode, indicating that more LiF was generated in the LC-HrGO. This finding could be attributed to the more defects on the LC-HrGO that can absorb more electrolytes and demonstrated rich LiF in the SEI, which has a low ion-diffusion barrier and a high Young's modulus for Li ion diffusion, thus resulting in fast kinetics for electrochemical reaction.^[35] The Li 1s (Figure 4b), C 1s, and O 1s (Figure S21) spectra with high Li_2CO_3 and organic components similarly demonstrated the above results. Due to more defects on the electrode, the Li ions in the electrolyte had a greater uniformity to be absorbed on LC-HrGO (Figure 4c and d). Considering the rich LiF in the SEI (Figure S22), Li ions can be transferred in the

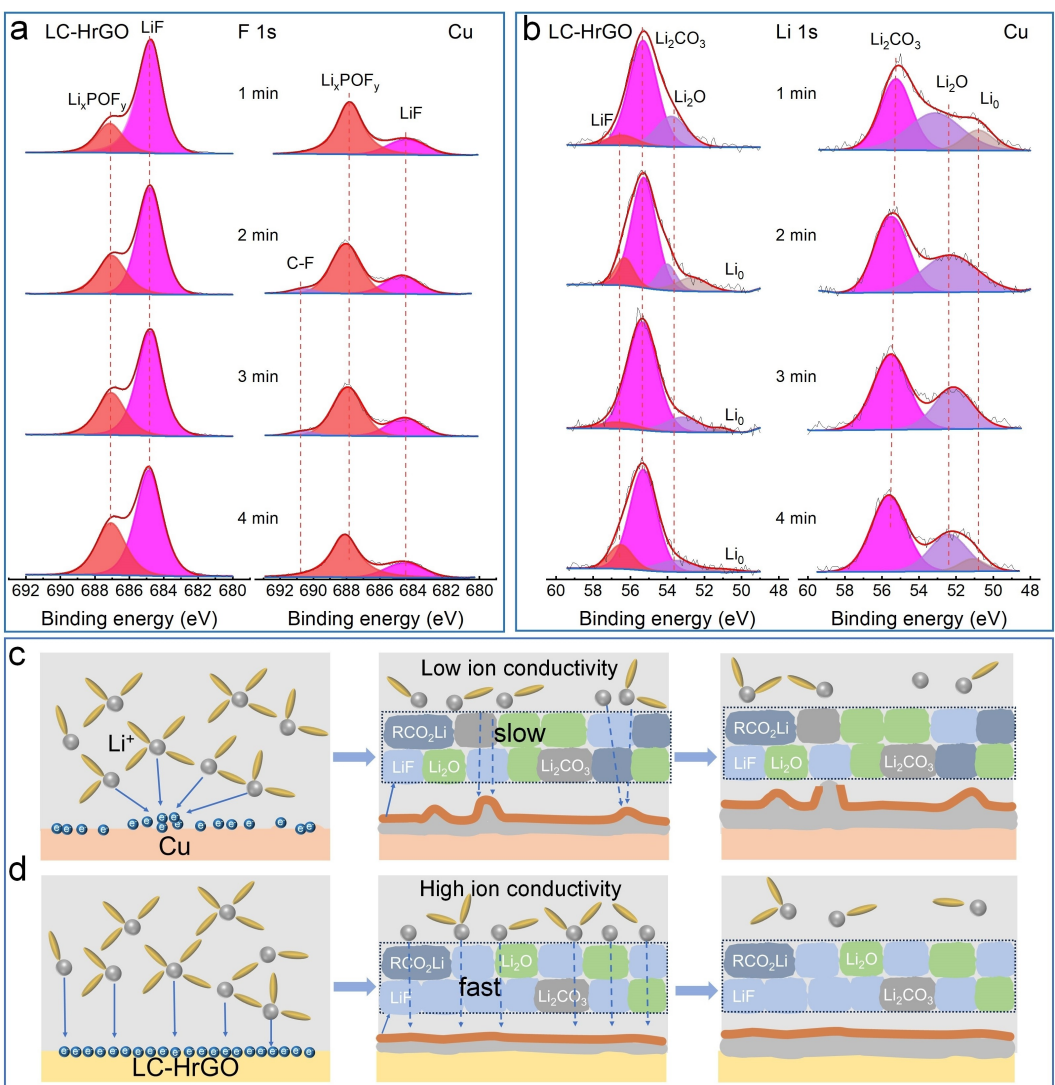


Figure 4. The XPS spectra of (a) F1s and (b) Li 1s of the SEI with Ar ion sputtering for different times formed on Cu foil and LC-HrGO electrodes after experienced 5 cycles, the mechanism of the Li ions from electrolyte plating then formed different SEI on the (c) Cu foil and (d) LC-HrGO.

SEI on LC-HrGO faster than that on the Cu electrode. Therefore, the LC-HrGO guides the uniform plating/stripping of Li metal.

The availability of the LC-HrGO-based AFLMBs was investigated. The cathode of LFP and the HrGO as anode current collector cells was prepared and then assembled with corresponding electrolytes to form Cu||LFP, HrGO||LFP, and LC-HrGO||LFP batteries. The charge/discharge curves of these anode-free batteries are shown in Figure 5a. The voltage profiles of the batteries at the discharge process were ~3.45 V according to the discharging potential of LFP. The LC-HrGO||LFP showed a high discharge specific capacity of 149.8 mAh g⁻¹ and high Coulombic efficiency of 98.3% at first cycle. However, the Cu||LFP and HrGO||LFP batteries showed lower specific capacities of 118.1 and 120.5 mAh g⁻¹, respectively. And the low Coulombic efficiency of the two cells also can be seen. The result may be attributed to the Li ions from the electrolyte that could be smoothly transported across the SEI on the surface of LC-HrGO. In addition, the stable SEI could demonstrate low

impedance. They corresponded with the CV profiles shown in Figure 5b. The CV curves of the cells can be used to evaluate the plating and stripping behavior of Li metal on the current collectors. The LC-HrGO||LFP cell displayed a smaller interval hysteresis of 0.32 V, which suggested milder polarization, than the Cu||LFP and HrGO||LFP cells with interval hysteresis between reduction and oxidation peaks of 0.43 and 0.46 V, respectively. The polarization suggested that the Li metal plating and stripping on LC-HrGO may demonstrate stable cycle performances of anode-free cells. The cycle performances of the cells (Figure 5c) indicated obviously different stability. The LC-HrGO||LFP cell maintained a high discharge specific capacity even after 100 cycles, whereas the Cu||LFP and HrGO||LFP cells showed rapid failure after less than 20 cycles. This finding suggested a considerable potential to fabricate AFLMBs by using LC-HrGO as current collectors. Furthermore, other cathodes, such as NCM 811, can be employed for AFLMBs on the

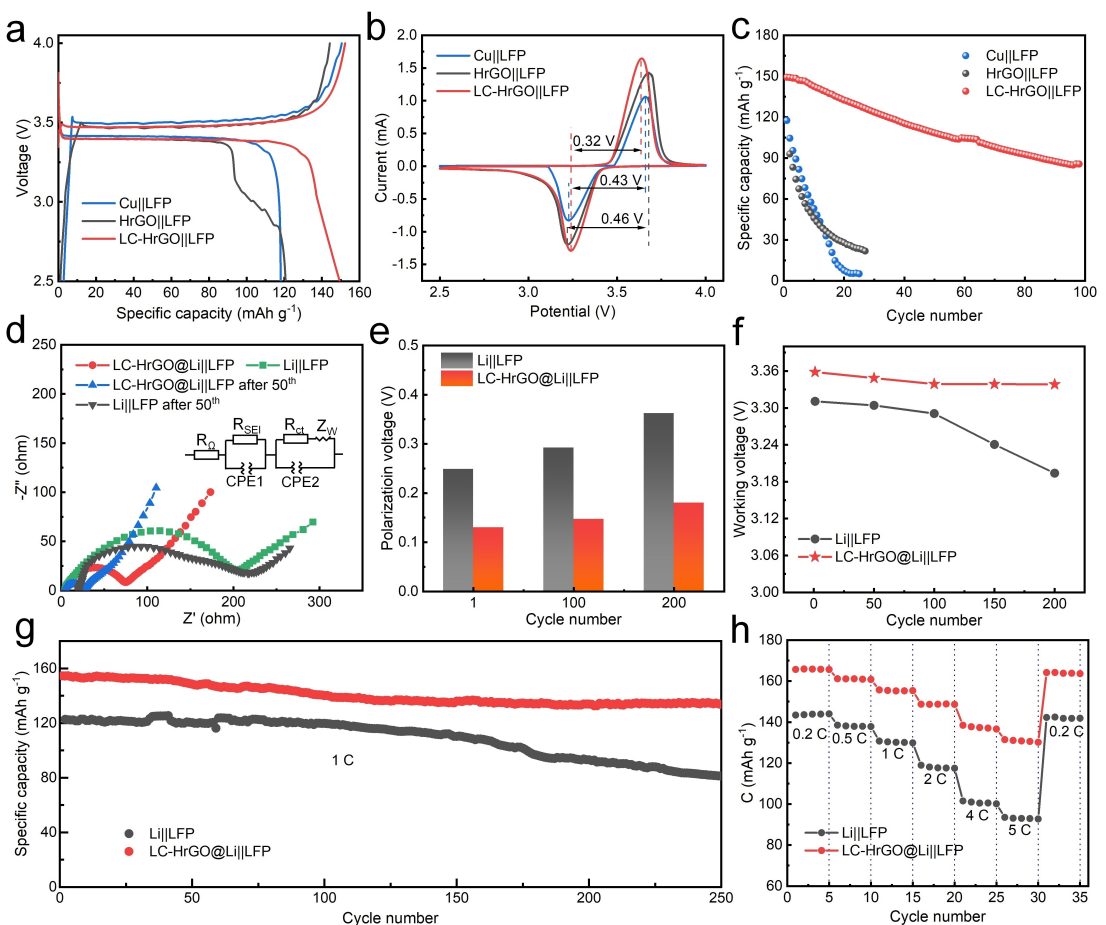


Figure 5. The electrochemical performances of the obtained AFLMBs and ALLMBs. (a) the charging and discharging curves, (b) CV curves and (c) cycle performances of the AFLMBs based on LC-HrGO and other current collectors at 0.2 C, (d) the EIS of different ALLMBs before and after cycling, the (e) polarization voltage and (f) working voltage of the ALLMBs based on LC-HrGO@Li, the (g) cycle performances and (h) C-rate performances of the ALLMBs based on LC-HrGO@Li anode.

basis of LC-HrGO with relative stable specific capacity with long cycles (Figure S23).

The LC-HrGO was first plated with 6 mAh cm^{-2} Li metal and then assembled to cells for electrochemical performance measurement to further improve the stability of ALLMBs. The Nyquist plots of the anode-less cell before cycling was investigated to explore the impedance behavior at a specific frequency. The results in Figure 5d showed that the anode-less LC-HrGO@Li battery had lower impedances than the bare Li in all frequency, indicating fast Li ion transfer at electrochemical reaction in LC-HrGO@Li || LFP. After 50 cycles, the interface impedance for LC-HrGO@Li || LFP further decreased, suggesting uniform and stable SEI layer formed in the electrode. And the increased interface impedance for the Li || LFP indicates dead Li and unstable SEI occurred. The obtained ALLMB based on LC-HrGO@Li showed a stable charging and discharging plateau even after 200 cycles (Figure S24). The cell displayed a specific capacity of approximately 140 mAh g^{-1} even after 200 cycles. However, the Li || LFP without LC-HrGO experienced severe capacity degradation during cycling, and its specific capacity decreased to $\sim 91 \text{ mAh g}^{-1}$ after similar cycles. In accordance with the charging/discharging curves, the polarization voltages

between the charging and discharging plateau of the LC-HrGO@Li || LFP and Li || LFP were compared (Figure 5e). The low polarization voltage of the cell based on the LC-HrGO demonstrated efficient electrochemical kinetic reaction. However, the sudden increase in the polarization of the Li || LFP suggested difficult transport for electrons and ions. Therefore, the same cathode indicated different specific capacity for the cells. Moreover, the stable working voltage from the charging/discharging curves demonstrated high energy density (Figure 5f). The cycle performances of ALLMBs were measured. The LC-HrGO@Li || LFP cell indicated a stable specific capacity of 134.5 mAh g^{-1} at 1 C even after 250 cycles, whereas the Li || LFP cell showed rapid failure from the beginning and after 250 cycles (Figure 5g), possibly due to the slow ion transfer, dendrites, or large plating of dead Li. The HrGO plated 6 mAh cm^{-2} Li for HrGO@Li || LFP also indicated sharply decreased capacity (Figure S25). The uneven plating and striping maybe the main reasons for the poor electrochemical performance. The high mass loading cathode and less electrolyte addition strategy according to our previous study also have been employed to evaluate the advantage of the LC-HrGO || LFP.^[6] The results indicated the excellent volume and mass

energy density based on the LC-HrGO (Figure S26, Table S7). In addition, the C-rate performance of ALLMBs was explored (Figure 5h). The specific capacity of Li||LFP significantly decreased with the increase in C-rates. The fading capacity could be attributed to its high resistance to Li ion diffusion, which resulted in slow kinetics.^[36] However, the LC-HrGO@Li||LFP battery showed a high specific capacity of 130.1 mAhg⁻¹ even at 5 C, which may be due to the homogenous SEIs formed on the anode with a high modulus and low diffusion barrier that enhanced the transport of ions from cathode to anode, even at high C-rate.^[37] In addition, the LiC₆ tends to induce Li plating on the electrode uniformly. The dendrite issue can be effectively alleviated by the LC-HrGO with abundant defects and efficient conductive network. Such a high-capacity retention clearly suggested that ALLMBs based on LC-HrGO@Li hold great advantages for fast charging/discharging in special environments.

Conclusions

In conclusion, we developed a facile process to directly fabricate LiC₆ in HrGO as a current collector by metallurgical technology. Combined with rich LiF phase formation in the SEI, more opportunities for Li ions from the electrolyte were available for coordination with LC-HrGO owing to the homogenous plating sites and favorable conductivity. The Li metal plating with reduced nucleation barrier was facilitated, which resulted in an enhanced kinetic condition. The assembled AFLMBs employing LC-HrGO as the current collector showed a capacity retention of 60% after 100 cycles. The corresponding ALLMBs indicated a stable specific capacity of 134.5 mAhg⁻¹ even after 250 cycles, with a remarkable rate capacity of 130.1 mAhg⁻¹ at 5 C. This work provides a substantial platform to develop anode-free and anode-less technologies that could significantly promote further development and commercialization of safe Li metal batteries.

Acknowledgements

This work was supported by the National Natural Science Foundation of China (22179055, 51861009) and the Department of Science and Technology of Jiangxi Province (JXSQ2019201037 and 20212BDH81013).

Conflict of Interests

The authors declare no conflicts of interest.

Data Availability Statement

The experimental details, other characterizations and electrochemical measurements are available in the Supporting Information.

Keywords: Anode-free · Anode-less · Li-metal batteries · Lithiated graphene · Current collector

- [1] X. Yuan, B. Liu, M. Mecklenburg, Y. Li, *Nature* **2023**, *620*, 86–91.
- [2] T. Naren, G. C. Kuang, R. Jiang, P. Qing, H. Yang, J. Lin, Y. Chen, W. Wei, X. Ji, L. Chen, *Angew. Chem. Int. Ed.* **2023**, *62*, e202305287.
- [3] F. Qiu, X. Li, H. Deng, D. Wang, X. Mu, P. He, H. Zhou, *Adv. Energy Mater.* **2019**, *9*, 1803372.
- [4] O. Lohrberg, K. Voigt, S. Maletti, H. Auer, K. Nikolowski, C. Heubner, A. Michaelis, *Adv. Funct. Mater.* **2023**, *33*, 2214891.
- [5] P. Molaiyan, M. Abdollahifar, B. Boz, A. Beutl, M. Krammer, N. Zhang, A. Tron, M. Romio, M. Ricci, R. Adelung, A. Kwade, U. Lassi, A. Paolella, *Adv. Funct. Mater.* **2023**, *34*, 2311301.
- [6] Y. Q. Mi, W. Deng, C. He, O. Eksik, Y. P. Zheng, D. K. Yao, X. B. Liu, Y. H. Yin, Y. S. Li, B. Y. Xia, Z. P. Wu, *Angew. Chem. Int. Ed.* **2023**, *135*, e202218621.
- [7] K. Park, J. Song, K. T. Lee, *Batteries & Supercaps* **2023**, *6*, e202300344.
- [8] W. Beichel, J. Skrotzki, P. Klose, C. Njel, B. Butschke, S. Burger, L. Liu, R. Thomann, Y. Thoman, D. Biro, S. Thiele, I. Krossing, *Batteries & Supercaps* **2022**, *5*, e202100347.
- [9] L. Hu, J. Wang, K. Wang, Z. Gu, Z. Xi, H. Li, F. Chen, Y. Wang, Z. Li, C. Ma, *Nat. Commun.* **2023**, *14*, 3807.
- [10] P. Shi, J. Ma, M. Liu, S. Guo, Y. Huang, S. Wang, L. Zhang, L. Chen, K. Yang, X. Liu, Y. Li, X. An, D. Zhang, X. Cheng, Q. Li, W. Lv, G. Zhong, Y. B. He, F. Kang, *Nat. Nanotechnol.* **2023**, *18*, 1–9.
- [11] Z. Ren, J. Li, Y. Gong, C. Shi, J. Liang, Y. Li, C. He, Q. Zhang, X. Ren, *Energy Storage Mater.* **2022**, *51*, 130–138.
- [12] Z. Y. Wang, Z. X. Lu, W. Guo, Q. Luo, Y. H. Yin, X. B. Liu, Y. S. Li, B. Y. Xia, Z. P. Wu, *Adv. Mater.* **2021**, *33*, 2006702.
- [13] H. Chen, Y. Yang, D. T. Boyle, Y. K. Jeong, R. Xu, L. S. de Vasconcelos, Z. Huang, H. Wang, H. Wang, W. Huang, H. Li, J. Wang, H. Gu, R. Matsumoto, K. Motohashi, Y. Nakayama, K. Zhao, Y. Cui, *Nat. Energy* **2021**, *6*, 790–798.
- [14] T. Chen, J. You, R. Li, H. Li, Y. Wang, C. Wu, Y. Sun, L. Yang, Z. Ye, B. Zhong, Z. Wu, X. Guo, *Adv. Sci.* **2022**, *9*, 2203216.
- [15] J. Zhang, H. Chen, M. Wen, K. Shen, Q. Chen, G. Hou, Y. Tang, *Adv. Funct. Mater.* **2022**, *32*, 2110110.
- [16] F. Cheng, X. Yang, O. Ka, L. Wen, X. Wang, W. Lu, *J. Mater. Chem. A* **2023**, *11*, 4205–4219.
- [17] W. Shin, A. Manthiram, *ACS Appl. Mater. Interfaces* **2022**, *14*, 17454–17460.
- [18] Y. Fan, J. Liao, D. Luo, Y. Huang, F. Sun, J. Nan, *Chem. Eng. J.* **2023**, *453*, 139903.
- [19] Y. Gao, X. Du, Z. Hou, X. Shen, Y. W. Mai, J. M. Tarascon, B. Zhang, *Joule* **2021**, *5*, 1860–1872.
- [20] B. Delley, *J. Phys. Chem.* **1996**, *100*, 6107–6110.
- [21] J. P. Perdew, K. Burke, M. Ernzerhof, *Phys. Rev. Lett.* **1996**, *77*, 3865.
- [22] M. Kunaseth, P. Poldorn, A. Junkeaw, J. Meeprasert, C. Rungrim, S. Namuangruk, N. Kungwan, C. Inntam, S. Jungsuttiwong, *Appl. Surf. Sci.* **2017**, *396*, 1712–1718.
- [23] K. Li, N. Li, N. Yan, T. Wang, Y. Zhang, Q. Song, H. Li, *Appl. Surf. Sci.* **2020**, *515*, 146028.
- [24] P. Xie, Y. Peng, X. B. Liu, B. Yang, F. Yang, H. J. Zhao, S. Y. Attia, X. Xu, Y. Sun, Y. H. Yin, Y. S. Li, Z. P. Wu, *Chem. Eng. J.* **2023**, *478*, 147304.
- [25] F. Yang, P. Xie, X. B. Liu, H. J. Zhao, T. Liu, Y. H. Yin, Y. S. Li, Z. P. Wu, *Carbon* **2023**, *214*, 118380.
- [26] Y. J. Shao, H. C. Wang, Z. L. Gong, D. W. Wang, B. Z. Zheng, J. P. Zhu, Y. X. Lu, Y. S. Hu, X. X. Guo, H. Li, X. J. Huang, Y. Yang, C. W. Nan, L. Q. Chen, *ACS Energy Lett.* **2018**, *3*, 1212.
- [27] Q. Zhang, Q. Wei, K. Huang, Z. Liu, W. Ma, Z. Zhang, Y. Zhang, H. M. Cheng, W. Ren, *Natl. Sci. Rev.* **2023**, *10*, nwad147.
- [28] Y. Liu, Q. Sun, P. Yu, Y. Wu, L. Xu, H. Yang, M. Xie, T. Cheng, W. A. Goddard III, *J. Phys. Chem. Lett.* **2021**, *12*, 2922–2929.
- [29] D. Lin, Y. Liu, Z. Liang, H. W. Lee, J. Sun, H. Wang, K. Yan, J. Xie, Y. Cui, *Nat. Nanotechnol.* **2016**, *11*, 626–632.

- [30] X. Nie, A. Zhang, Y. Liu, C. Shen, M. Chen, C. Xu, Q. Liu, J. Cai, A. Alfaraidi, C. Zhou, *Energy Storage Mater.* **2019**, *17*, 341–348.
- [31] P. Shi, T. Li, R. Zhang, X. Shen, X. B. Cheng, R. Xu, J. Q. Huang, X. R. Chen, H. Liu, Q. Zhang, *Adv. Mater.* **2019**, *31*, 1807131.
- [32] H. Lim, S. Jun, Y. B. Song, K. H. Baeck, H. Bae, G. Lee, J. Kim, Y. S. Jung, *Adv. Energy Mater.* **2024**, 2303762.
- [33] S. Ye, L. Wang, F. Liu, P. Shi, H. Wang, X. Wu, Y. Yu, *Adv. Energy Mater.* **2020**, *10*, 2002647.
- [34] H. Wang, H. Cheng, D. Li, F. Li, Y. Wei, K. Huang, B. Jiang, H. Xu, Y. Huang, *Adv. Energy Mater.* **2023**, *13*, 2204425.
- [35] P. Bai, X. Ji, J. Zhang, W. Zhang, S. Hou, H. Su, M. Li, T. Deng, L. Cao, S. Liu, X. He, Y. Xu, C. Wang, *Angew. Chem. Int. Ed.* **2022**, *61*, e202202731.
- [36] A. Hu, F. Li, W. Chen, T. Lei, Y. Li, Y. Fan, M. He, F. Wang, M. Zhou, Y. Hu, Y. Yan, B. Chen, J. Zhu, J. Long, X. Wang, J. Xiong, *Adv. Energy Mater.* **2022**, *12*, 2202432.
- [37] X. J. Hu, Y. P. Zheng, Z. W. Li, C. Xia, D. H. C. Chua, X. Hu, T. Liu, X. B. Liu, Z. P. Wu, B. Y. Xia, *Angew. Chem. Int. Ed.* **2024**, *63*, e202319600.

Manuscript received: March 3, 2024
Revised manuscript received: May 30, 2024
Accepted manuscript online: June 3, 2024
Version of record online: July 18, 2024